Macromolecules
ARTICLE

Macromolecules **2010**, *43*, 1387–1395 **1387**
DOI: 10.1021/ma902309a

Compartmentalization in Atom Transfer Radical Polymerization to High Conversion in Dispersed Systems: Effects of Diffusion-Controlled Reactions

Per B. Zetterlund*

Centre for Advanced Macromolecular Design (CAMD), School of Chemical Sciences and Engineering, The University of New South Wales, Sydney NSW 2052, Australia

Received October 16, 2009; Revised Manuscript Received January 6, 2010

ABSTRACT: Effects of diffusion control in a compartmentalized atom transfer radical polymerization (ATRP) system have been investigated by modeling and simulations employing modified Smith−Ewart equations in connection with conversion-dependent rate coefficients for the system styrene/polystyrene-Cl/CuCl/4,4′-di(5-nonyl)-2,2′-bipyridine (dNbpy) at 75 °C. The effects of conversion-dependent rate coefficients for deactivation (k_{deact}) and termination (k_t) were investigated in detail for the particle diameter 30 nm, i.e., a strongly compartmentalized system. The decrease in k_{deact} at high conversion results in an increase in the number of monomer units added per activation−deactivation cycle, thereby causing slight loss of control relative to when k_{deact} remains constant. The conversion dependence of k_t results in a minor increase in livingness at high conversion relative to when k_t remains constant. The individual compartmentalized rates of deactivation and termination have been analyzed in detail based on the particle distributions N_i^j, where N_i^j is the number of particles containing i propagating radicals and j deactivator species.

Introduction

Controlled/living radical polymerization (CLRP)[1] is now a well-established area of research, and recent years have seen a gradual shift from mainly fundamental research on CLRP in homogeneous systems toward implementation in various dispersed systems[2−5] as well as a range of other more specific synthetic applications of CLRP.[6,7] Polymerization in dispersed systems can be considerably more complex than the homogeneous counterparts due to various features such as phase transfer events, interface effects, and compartmentalization, which can significantly alter the progression of the polymerization.

Compartmentalization refers to the physical isolation of reactants in discrete confined spaces, i.e., the monomer droplets or polymer particles. There are two separate effects of compartmentalization: the segregation effect and the confined space effect.[2,8] The segregation effect refers to how two species in different particles are unable to react, whereas the confined space effect refers to the rate of reaction between two species being higher in a small particle than in a large particle. CLRP systems that operate based on the persistent radical effect,[9] e.g., nitroxide-mediated radical polymerization (NMP)[1,10] and atom transfer radical polymerization (ATRP),[1,11,12] may experience both the confined space effect on deactivation (increase in deactivation rate) and the segregation effect on termination (decrease in termination rate); i.e., both propagating radicals and deactivator species may be compartmentalized. In systems that rely on degenerative transfer, e.g., reversible addition−fragmentation chain transfer (RAFT) polymerization,[13,14] termination can be affected by compartmentalization,[15,16] but the activation−deactivation process is not because the concentration of dormant chains (e.g., RAFT end groups) is normally too high. In NMP[8,17−20] and ATRP,[21,22] compartmentalization can thus potentially be exploited to improve control and livingness at the cost of a lower polymerization rate (R_p), whereas in RAFT, the livingness can be improved with an accompanying increase in R_p. However, if the deactivator is sufficiently water-soluble in NMP[23,24] and ATRP,[25] there will be no confined space effect on deactivation.

The most convincing experimental evidence of compartmentalization in ATRP so far has been reported by Simms and Cunningham,[26,27] who found that very high molecular weights (M_n = 989 900, M_w/M_n = 1.25) were obtained in the redox-initiated reverse ATRP of *n*-butyl methacrylate in miniemulsion. Such high molecular weights cannot be attained with good control (low M_w/M_n) based on current understanding of ATRP in the absence of compartmentalization effects. Experimental data consistent with compartmentalization effects in miniemulsion NMP have been obtained by Cunningham and co-workers for 2,2,6,6-tetramethylpiperidine-*N*-oxyl (TEMPO)-mediated miniemulsion polymerization of styrene (St)[28] as well as by Okubo and Zetterlund in microemulsion NMP of St using TEMPO[29] and *N*-*tert*-butyl-*N*-[1-diethylphosphono-(2,2-dimethylpropyl)] nitroxide (SG1).[30]

In the case of ATRP in bulk, termination is diffusion-controlled from zero conversion onward,[31−33] and depending on the specific system and conditions, it is likely that propagation[34,35] and deactivation[35,36] come under diffusion control at intermediate/high conversion. The ATRP activation reaction is not likely to be significantly influenced by reactant diffusion due to the low value of the chemical reaction rate coefficient.[1] It has recently been reported that effects of diffusion control are weak in the case of TEMPO-mediated polymerization of St.[37]

To date, the effects of compartmentalization to high conversion in ATRP (and NMP) have not been investigated. In this work, this deficiency is redressed by use of modeling and simulations based on previously employed modified Smith−Ewart equations[21,22] in connection with conversion-dependent rate coefficients for the ATRP system St/polystyrene-Cl/CuCl/4,4′-di(5-nonyl)-2,2′-bipyridine (dNbpy) at 75 °C in bulk.

*Tel +61 2 9385 4331; Fax +61 2 9385 6250; e-mail p.zetterlund@unsw.edu.au.

Published on Web 01/13/2010

Table 1. Rate Coefficients Employed in the Simulations

	St/CuCl/dNbpy/75 °C
k_{act} (s^{-1})	1.66×10^{-3} [a]
k_{deact} (M^{-1} s^{-1})	conversion-dependent or 4.3×10^{6} [b]
k_p (M^{-1} s^{-1})	566[c]
k_t (M^{-1} s^{-1})	conversion-dependent or 1.22×10^{8} [d]
$k_{i,th}$ (M^{-2} s^{-1})	1.12×10^{-12} [e]

[a] Based on k_{act}(1-phenylethyl chloride/dNbpy) = 5.6×10^{-5} at 35 °C and k_{act}(1-phenylethyl chloride/dHbpy/toluene) = 0.018 at 110 °C (dHbpy = 4,4′-diheptyl-2,2′-bipyridine), giving E_{act} = 75.5 kJ mol^{-1} and $A_{act} = 3.56 \times 10^{8}$ s^{-1}.[38] [b] k_{deact} for phenylethyl radical and $CuCl_2$/dNbpy in acetonitrile.[38] [c] Reference 46. [d] Reference 52 (based on termination rate = $2k_t[P^\bullet]^2$). [e] Reference 39 (based on radical generation rate = $k_{i,th}[St]^3$).

Model Development

Bulk. Bulk ATRP was modeled based on eqs 1−5:[12,38]

$$\frac{d[M]}{dt} = -k_p[P^\bullet][M] \quad (1)$$

$$\frac{d[PCl]}{dt} = k_{deact}[P^\bullet][CuCl_2] - k_{act}[PCl][CuCl] \quad (2)$$

$$\frac{d[CuCl]}{dt} = k_{deact}[P^\bullet][CuCl_2] - k_{act}[PCl][CuCl] \quad (3)$$

$$\frac{d[CuCl_2]}{dt} = k_{act}[PCl][CuCl] - k_{deact}[P^\bullet][CuCl_2] \quad (4)$$

$$\frac{d[P^\bullet]}{dt} = k_{act}[PCl][CuCl] + k_{i,th}[M]^3 - k_{deact}[P^\bullet][CuCl_2] - 2k_t[P^\bullet]^2 \quad (5)$$

where M, PCl, and $P^\bullet$ are monomer, alkyl chloride, and propagating radical, respectively, and k_p, k_{act}, k_{deact}, $k_{i,th}$, and k_t are rate coefficients for propagation, activation, deactivation, thermal (spontaneous) initiation of St,[39,40] and termination, respectively. The values of the rate coefficients employed in the simulations are listed in Table 1. The "2" corresponding to the fact that each thermal initiation event of St generates two radicals is included in the value of $k_{i,th}$. The number of monomer units added per activation−deactivation cycle (N) was computed via eq 6:

$$N = \frac{k_p[P^\bullet][M]}{k_{deact}[P^\bullet][CuCl_2]} = \frac{k_p[M]}{k_{deact}[CuCl_2]} \quad (6)$$

The equations were implemented and solved using the software VisSim (version 6.0A11, Visual Solutions Inc.).

Compartmentalization. Compartmentalization in ATRP was modeled using the previously published approach based on a modified Smith−Ewart equation[41] that accounts for compartmentalization of both $P^\bullet$ and $CuCl_2$:[21,22]

$$\frac{dN_i^j}{dt} = N_A v_p k_{act}[PCl][CuCl](N_{i-1}^j - N_i^j) + 0.5k_{i,th}[M]^3 N_A v_p\{N_{i-2}^j - N_i^j\} + \frac{k_t}{N_A v_p}\{(i+2)(i+1)N_{i+2}^j - (i)(i-1)N_i^j\} + \frac{k_{deact}}{N_A v_p}\{(i+1)(j+1)N_{i+1}^{j+1} - (i)(j)N_i^j\} \quad (7)$$

where N_i^j is the number of particles containing i $P^\bullet$ and j $CuCl_2$, v_p is the particle volume, and N_A is Avogadro's number. The average numbers of $P^\bullet$ ($\bar{n}_{P^\bullet}$) and $CuCl_2$ ($\bar{n}_{CuCl_2}$) per particle are

$$\bar{n}_{P^\bullet} = \frac{1}{N_p}\sum_i\sum_j iN_i^j \quad (8)$$

$$\bar{n}_{CuCl_2} = \frac{1}{N_p}\sum_i\sum_j jN_i^j \quad (9)$$

where $N_p = \sum_i\sum_j N_i^j$ (the total number of particles). The overall concentrations of $P^\bullet$ and $CuCl_2$ in the organic phase are

$$[P^\bullet] = \frac{\bar{n}_{P^\bullet}}{N_A v_p} \quad (10)$$

$$[CuCl_2] = \frac{\bar{n}_{CuCl_2}}{N_A v_p} \quad (11)$$

The propagation step is not affected by compartmentalization (because each particle contains a very high number of monomer units, i.e., no confined space effect[17]), and therefore eqs 1 and 10 can be used to compute the monomer conversion. This also applies to the activation reaction between PCl and CuCl—both reactants are present in high concentration. The concentrations of PCl and CuCl are thus given by

$$\frac{d[PCl]}{dt} = \frac{d[CuCl]}{dt} = \frac{k_{deact}}{(N_A v_p)^2 N_p}\sum_i\sum_j ijN_i^j - k_{act}[PCl][CuCl] \quad (12)$$

The number of monomer units added per activation−deactivation cycle (N) was computed via eq 13:

$$N = \frac{k_p[M][P^\bullet]}{\frac{k_{deact}}{(N_A v_p)^2 N_p}\sum_i\sum_j ijN_i^j} \quad (13)$$

The equations were implemented and solved using the software VisSim employing numerical integration (backward Euler integration algorithm[42]) with a step size of 1 s. In all simulations (including bulk), the initial concentrations were $[PCl]_0 = [CuCl]_0 = 0.0181$ M and [M] = 8.7 M. The model corresponds to an ideal miniemulsion polymerization, initially comprising monomer droplets that are subsequently converted to polymer particles. The number of monomer droplets (polymer particles) remains constant; i.e., there is no secondary nucleation, Ostwald ripening,[43] or coagulation. It has been assumed that phase transfer events such as exit and subsequent entry of deactivator and small radicals generated by chain transfer to monomer do not occur to make the phenomenon of compartmentalization more tractable. However, it cannot be excluded that such events may in fact to some extent influence a real system.[2,25]

Diffusion-Controlled Reactions. The concept of diffusion control is perhaps best illustrated via eq 14, derived from the so-called encounter-pair model:[44]

$$\frac{1}{k} = \frac{1}{k_{chem}} + \frac{1}{k_{diff}} \quad (14)$$

where k denotes the overall rate coefficient for a bimolecular reaction, and k_{chem} and k_{diff} are the corresponding rate

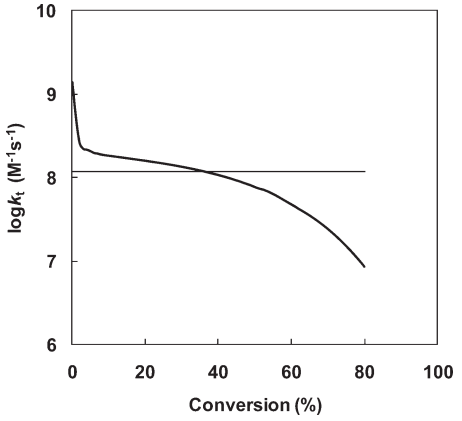

Figure 1. Thick line: experimentally obtained k_t vs conversion for RAFT polymerization of styrene in bulk at 80 °C with $M_{n,th}$ (100% conversion) = 44 000 g mol^{-1}.[48] Thin line: $k_t = 1.2 \times 10^8$ M^{-1} s^{-1}.

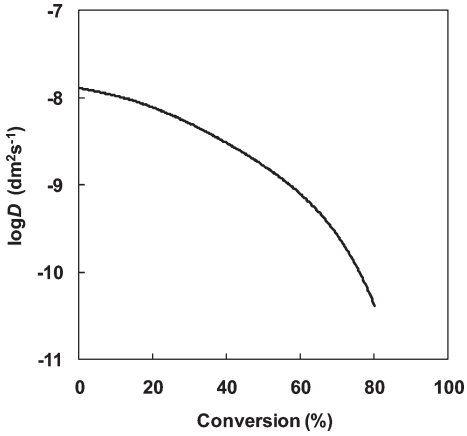

Figure 2. Estimated diffusion coefficient of the Cu(II) complex $CuCl_2$/2dNbpy in bulk St as a function of St conversion at 75 °C. See text for details.

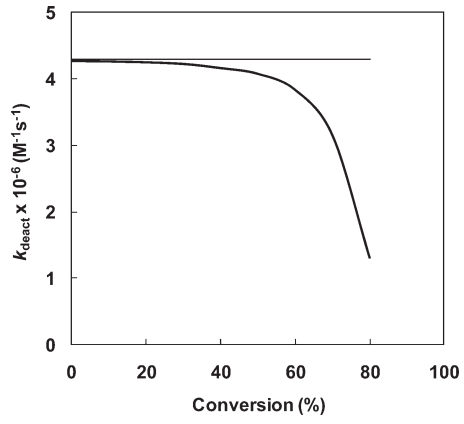

Figure 3. Thick line: estimated deactivation rate coefficient for the ATRP system $CuCl_2$/2dNbpy/St/75 °C as a function of St conversion (see text for details). Thin line: $k_{deact} = 4.3 \times 10^6$ M^{-1} s^{-1}.

coefficients for the chemical and diffusive steps, respectively. Equation 14 is derived by assuming that the overall reaction time is the sum of the diffusive step and the chemical reaction step. The more rapid the chemical step, the more likely is a reaction to come under diffusion control as the viscosity increases when the polymerization proceeds.

In the present study of the ATRP system St/polystyrene-Cl/CuCl/dNbpy at 75 °C in bulk, simulations were carried out to 80% St conversion. The value of k_p has been experimentally determined as a function of conversion in the conventional bulk polymerization of styrene at 70 °C,[34,45] revealing that k_p remains approximately constant to 80% conversion. Therefore, the IUPAC benchmark low conversion k_p value[46] of 566 M^{-1} s^{-1} was employed at all conversions. The dependence of k_t on both conversion and propagating radical chain length[47] (the propagating radical chain length increases with conversion in CLRP) was captured by employing experimental data for the RAFT polymerization of styrene in bulk at 80 °C (Figure 1).[48] Inherent in this approach is that the value of k_t for spontaneously generated radicals from styrene will be somewhat underestimated (because at nonzero conversions, k_t of the experimental data in Figure 1 corresponds to higher molecular weights than the spontaneously generated radicals as governed by the evolution of M_n with conversion in CLRP).

The conversion dependence of k_{deact} was modeled (experimental conversion dependence not available) using, as a starting point, the experimental data reported by Faldi et al.[49] for the diffusion coefficient of methyl methacrylate (D_{MMA}) in a MMA/PMMA matrix at various polymer contents at 50 °C. The value of k_{diff} is given by the Smoluchowski equation:

$$k_{diff} = 4\pi N_A \sigma D_{Cu(II)} \quad (15)$$

The diffusion coefficient in eq 15 is strictly speaking the mutual diffusion coefficient, i.e., the sum of the respective self-diffusion coefficients of Cu(II) ($CuCl_2$) and P$^\bullet$. However, the diffusion coefficient of the Cu(II) complex is much larger than that of a propagating macroradical, and the use of $D_{Cu(II)}$ in eq 15 is thus an excellent approximation. The parameter σ is the collision radius, taken to be equal to the Lennard-Jones diameter of St at 6.0×10^{-10} m.[50] Values of $D_{Cu(II)}$ at 75 °C were obtained from the data reported by Faldi et al.[49] at 50 °C by assuming an activation energy of $D_{Cu(II)}$ of 3257 J mol^{-1} [49](independent of conversion). The Cu(II) complex $CuCl_2$/2dNbpy is considerably bulkier than MMA, and one would therefore expect $D_{Cu(II)} < D_{MMA}$. Reyniers et al.[51] found by free volume theory that D for the Cu(II) complex $CuBr_2$/*N,N,N′,N′,N″*-pentamethyldiethylenetriamine (PMDETA) is 21 times lower than D_{MMA} in MMA monomer at 25 °C. It was therefore assumed that $D_{Cu(II)}/D_{MMA}$(Faldi et al.) = 1/21 at all conversions in the present study. The resulting $D_{Cu(II)}$ vs conversion (Figure 2) was subsequently fitted with an empirical function and used in conjunction with eq 14 and $k_{deact,chem}$ (k_{chem}) = 4.3×10^6 M^{-1} s^{-1} [22] to compute k_{deact} (k in eq 14) as a function of conversion (Figure 3).

Results and Discussion

Diffusion Control in Bulk. Before considering the compartmentalized case, it is instructive to examine the effects of diffusion-controlled termination and deactivation in the ATRP system St/polystyrene-Cl/CuCl/dNbpy at 75 °C in bulk. Simulations were carried out based on eqs 1−6 using the conversion-dependent k_t (Figure 1) and k_{deact} (Figure 3) (case A) as well as, for comparison, using $k_t = 1.2 \times 10^8$ M^{-1} s^{-1} [52] and $k_{deact} = 4.3 \times 10^6$ M^{-1} s^{-1} (case B).[22]

The initial polymerization rate (R_p) is lower for case A (i.e., the propagating radical concentration is lower) due to the initially high value of k_t (Figure 4a). However, at intermediate to high conversion levels, R_p is higher for case A than case B due to the decreases in both k_t and k_{deact} with

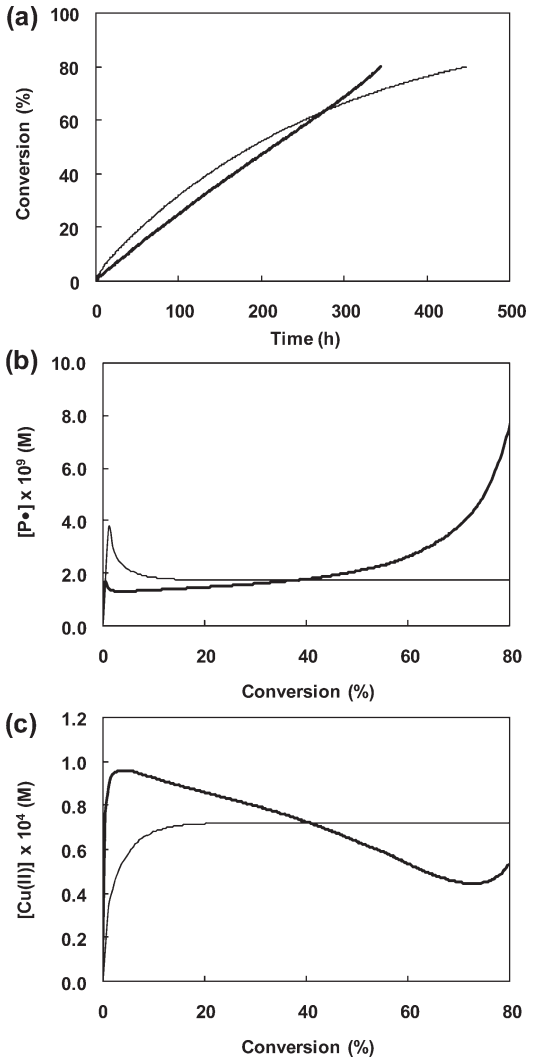

Figure 4. Simulated conversion−time (a), concentration of propagating radicals (b), and Cu(II) (c) for the ATRP system St/polystyrene-Cl/CuCl/dNbpy in bulk at 75 °C. Thick lines: case A, conversion-dependent k_t and k_{deact} (see text). Thin lines: case B, $k_t = 1.2 \times 10^8$ M^{-1} s^{-1} and $k_{deact} = 4.3 \times 10^6$ M^{-1} s^{-1}.

increasing conversion. These trends are also reflected in the propagating radical (Figure 4b) and deactivator (Cu(II)) concentrations (Figure 4c). The Cu(II) concentration is higher for case A at low to intermediate conversion due to the higher termination rate (termination "releases" Cu(II) by consumption of propagating radicals). The decrease in [Cu(II)] over much of the conversion range in case A is caused by the continuous reduction in k_t in combination with generation of new radicals via spontaneous initiation of St. The increase in [Cu(II)] at high conversion in case A is due to the decrease in k_{deact}. In case A, R_p is close to constant over a very wide conversion range because the gradual decrease in monomer concentration is offset by the increase in propagating radical concentration due to the decreases in both k_t and k_{deact}.

The livingness is evaluated in terms of the ratio $[PCl]/[PCl]_0$. It is noted that this definition of livingness includes the contribution toward [PCl] of the radicals from spontaneous initiation of styrene that ultimately result in PCl species. In case A, the gradual increase in $[PCl]/[PCl]_0$ over the intermediate conversion range is caused by radicals generated by spontaneous initiation of St that result in formation of new PCl species in combination with the

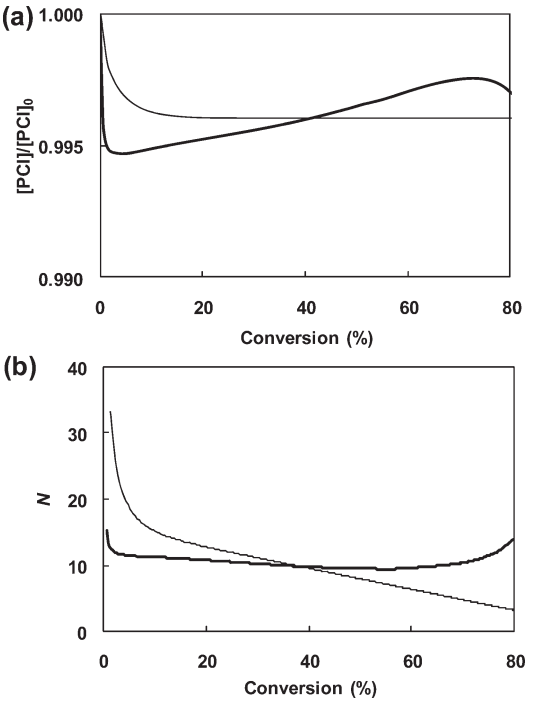

Figure 5. Simulated fractional livingness (a; expressed as [PCl] relative to its initial value) and number of monomer units added per activation−deactivation cycle (b; N) for the ATRP system St/polystyrene-Cl/CuCl/dNbpy in bulk at 75 °C. Thick lines: conversion-dependent k_t and k_{deact} (case A; see text). Thin lines: $k_t = 1.2 \times 10^8$ M^{-1} s^{-1} and $k_{deact} = 4.3 \times 10^6$ M^{-1} s^{-1} (case B).

gradual decrease in k_t (Figure 5a). The decrease in $[PCl]/[PCl]_0$ at high conversion is caused by increased termination due to the decrease in k_{deact}. For case B, the livingness initially decreases and then remains close to constant as a result of the increase in deactivator concentration with increasing conversion (the persistent radical effect[9]).

The degree of control over the MWD (value of M_w/M_n) can be assessed via examination of the number of propagation events per activation−deactivation cycle for an individual chain (N).[8] In ideal CLRP, that is, in the absence of termination, transfer, and other side reactions, M_w/M_n decreases with an increasing number of activation−deactivation cycles as polymer chains grow.[38] Thus, for a given MW, M_w/M_n decreases with decreasing N. In case A, there is a slight initial decrease, after which N remains close to constant over most of the conversion range, with a gentle increase at high conversion (Figure 5b). In case B, N initially decreases sharply, followed by a more gradual continuous decrease. These results are readily explained based on the changes in [M], [Cu(II)], and k_{deact} with conversion in accordance with eq 6.

From the above results it is thus apparent that the conversion dependences of k_t and k_{deact} exert significant influences on the present ATRP system in bulk.

Diffusion Control in Compartmentalized System. Figure 6 shows simulated conversion−time data to high conversion for St/polystyrene-Cl/CuCl/dNbpy in a dispersed system for various particle diameters and in bulk at 75 °C using the models with conversion-dependent k_t and k_{deact}. Overall, the behavior is qualitatively the same as previously reported in both ATRP[21,22] and NMP[8,17−19] at low conversion; i.e., R_p is lower than in bulk for sufficiently small particles but higher than in bulk for a certain particle size range. This general behavior has been explained in detail in previous reports and will not be repeated here.[8,17−19,21,22]

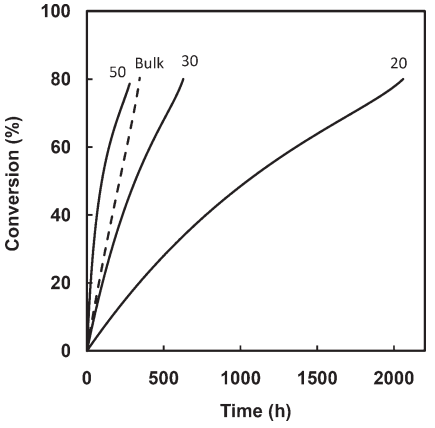

Figure 6. Simulated conversion−time data for the ATRP system St/polystyrene-Cl/CuCl/dNbpy in a dispersed system with particle diameters as indicated (nm) and in bulk (broken line) at 75 °C using models with conversion-dependent k_t and k_{deact} (case A; see text).

We next turn our attention to the specific effects of conversion dependence of k_t and k_{deact} in the dispersed system with $d = 30$ nm. Simulations were carried out using the conversion-dependent k_t and k_{deact} (case A) as well as, for comparison, using $k_t = 1.2 \times 10^8$ M^{-1} s^{-1} [52] and $k_{deact} = 4.3 \times 10^6$ M^{-1} s^{-1} (case B). Unlike the situation in bulk (Figure 4a), the conversion−time profiles were unaffected by the conversion dependences of k_t and k_{deact} until ∼60% conversion (Figure 7a). Beyond 60% conversion, R_p(case A) > R_p(case B). For conversions < 60%, k_{deact} remains relatively constant (Figure 3), whereas k_t decreases gradually with increasing conversion from the outset of the polymerization. It can thus be concluded that the decrease in k_{deact} is the main factor causing the increase in R_p (and $\bar{n}_{P\bullet}$) beyond 60% conversion and that k_t does not exert a significant influence (discussed further below). To confirm this, simulations were carried out with $k_t = 10^6$ M^{-1} s^{-1}, revealing only a negligible difference in R_p at low conversion compared to when $k_t = 1.2 \times 10^8$ M^{-1} s^{-1} (both simulations with $k_{deact} = 4.3 \times 10^6$ M^{-1} s^{-1}).

Consistent with the above, the values of $\bar{n}_{P\bullet}$ (Figure 7b) and $\bar{n}_{CuCl_2}$ (Figure 7c) are virtually identical for case A and case B up to ∼50−60% conversion. At high conversion, $\bar{n}_{P\bullet}$ increases for case A relative to case B due to the decrease in k_{deact} in case A. However, at high conversion, $\bar{n}_{CuCl_2}$(case B) > $\bar{n}_{CuCl_2}$(case A), despite k_{deact}(case B) > k_{deact}(case A). The main (by far) contribution toward $\bar{n}_{CuCl_2}$ comes from particles of the type N_0^2, i.e., particles of the type N_2^2 where a termination event has occurred. It follows that the reduction in k_t at high conversion in case A is what causes $\bar{n}_{CuCl_2}$(case B) > $\bar{n}_{CuCl_2}$(case A). The values of $\bar{n}_{P\bullet}$ are of the order of 10^{-5}, whereas $\bar{n}_{CuCl_2}$ does not increase beyond 0.25. In other words, the majority of particles contain no propagating radicals and no deactivator species at any given time (N_0^0).

The livingness is slightly higher for case A than case B at high conversion (Figure 8a) as a result of the lower value of k_t in that conversion range for case A. The decrease in k_{deact} at high conversion in case A results in an increase in N, i.e., in this conversion range control(case B) > control(case A) (Figure 8b).

Particle Distribution (N_i^j). In order to further analyze the inner workings of the compartmentalized system, it is instructive to examine the number fractions of the various particle types. Recall that N_i^j denotes the number of particles containing i P$^\bullet$ and j $CuCl_2$. Figure 9 shows plots of N_0^0, N_0^2, N_1^1, and N_2^2 vs conversion for $d = 30$ nm with conversion-dependent k_t and k_{deact} (case A) in the absence of spontaneous initiation. Spontaneous initiation was excluded from the simulations in Figure 9 to further simplify the situation, in particular with regards to the effects of compartmentalization on termination (discussed in detail later).

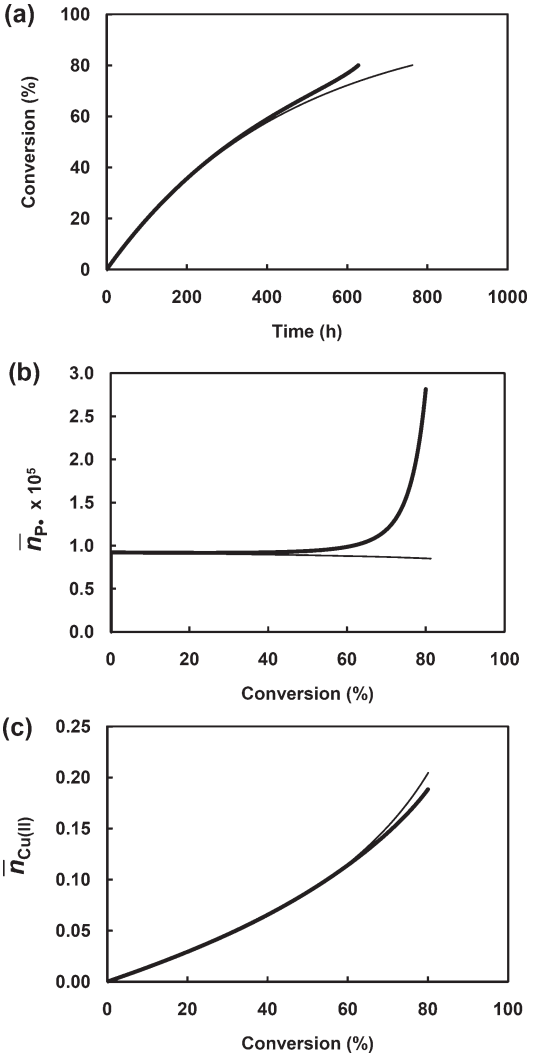

Figure 7. Simulated conversion−time (a), average number of propagating radicals per particle (b), and average number of Cu(II) per particle (c) for St/polystyrene-Cl/CuCl/dNbpy in a dispersed system with $d = 30$ nm at 75 °C. Thick lines: conversion-dependent k_t and k_{deact} (case A; see text). Thin lines: $k_t = 1.2 \times 10^8$ M^{-1} s^{-1} and $k_{deact} = 4.3 \times 10^6$ M^{-1} s^{-1} (case B).

The particle type present in the highest number is by far N_0^0, followed by N_0^2. The value of N_0^0 decreases gradually with conversion (but always makes up in excess of 90% of the particles,) as termination in particles N_2^2 results in a gradual increase in N_0^2. The particle types present in the highest number of relevance to deactivation (i.e., particles in which deactivation occurs) are N_1^1 and N_1^3 ($N_1^1 \gg N_1^3$ by ∼2 orders of magnitude). The particle types present in the highest number of relevance to termination (i.e., particles in which termination occurs) are N_2^2 and N_2^4 ($N_2^2 \gg N_2^4$ by ∼2 orders of magnitude). The significance of the particle distribution N_i^j will be discussed further below in relation to the compartmentalized rates of deactivation and termination.

Compartmentalization Effects on Deactivation and Termination. The separate effects of compartmentalization on deactivation and termination were analyzed by comparison of the "compartmentalized rates" (R^c) with the

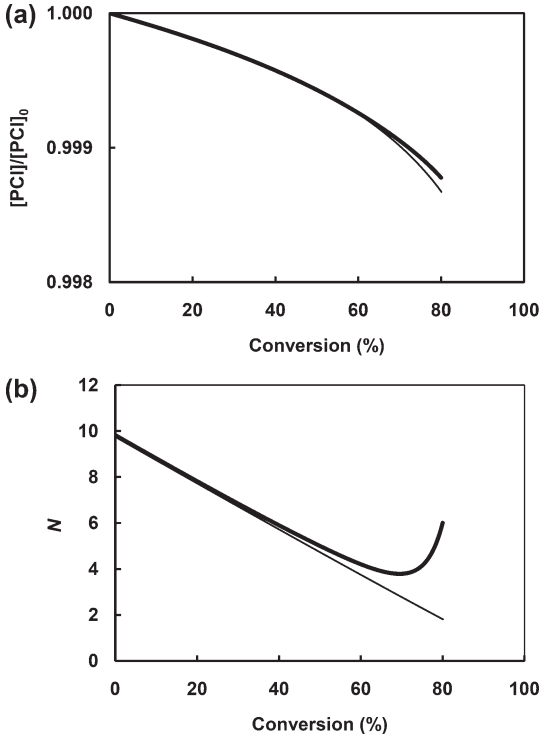

Figure 8. Simulated fractional livingness (a; expressed as [PCl] relative to its initial value) and number of monomer units added per activation−deactivation cycle (b; N) for St/polystyrene-Cl/CuCl/dNbpy in a dispersed system with $d = 30$ nm at 75 °C. Thick lines: conversion-dependent k_t and k_{deact} (case A; see text). Thin lines: $k_t = 1.2 \times 10^8$ M^{-1} s^{-1} and $k_{deact} = 4.3 \times 10^6$ M^{-1} s^{-1} (case B).

corresponding "noncompartmentalized rates" (R^{nc}) based on eqs 16−19:[8]

$$R_{deact}^{c} = \frac{k_{deact}}{(N_A v_p)^2 N_p} \frac{1}{\sum_i \sum_j ijN_i^j} \quad (16)$$

$$R_t^{c} = \frac{2k_t}{(N_A v_p)^2 N_p} \frac{1}{\sum_i \sum_j i(i-1)N_i^j} \quad (17)$$

$$R_{deact}^{nc} = k_{deact}[P^\bullet][CuCl_2] \quad (18)$$

$$R_t^{nc} = 2k_t[P^\bullet]^2 \quad (19)$$

using [P$^\bullet$] and [CuCl$_2$] from eqs 10 and 11, respectively. The value of R^{nc} is the rate that would be observed if all compartmentalization effects were "removed" instantaneously (i.e., if all particles were instantaneously combined to form a continuous organic phase). Thus, the noncompartmentalized system is not a real bulk system, but a hypothetical bulk system where the concentrations of P$^\bullet$ and $CuBr_2$ correspond to the overall instantaneous organic phase concentrations in a compartmentalized system.

Figure 10a shows $R_{deact}^{c}/R_{deact}^{nc}$ as a function of conversion. The values of $R_{deact}^{c}/R_{deact}^{nc}$ decrease with increasing conversion, but $R_{deact}^{c}/R_{deact}^{nc} > 1$ throughout the conversion range investigated. The higher deactivation rate in the compartmentalized system is due to the confined space effect, whereby [CuCl$_2$] is higher in a particle containing CuCl$_2$ than in the corresponding bulk system; i.e., some particles do not contain any CuCl$_2$ ($\bar{n}_{CuCl_2} < 1$).[17,19,22] The magnitude of the confined space effect decreases dramatically with increasing conversion as a consequence of $\bar{n}_{CuCl_2}$ increasing with conversion (Figure 7c). The effects of the conversion dependences of k_t and k_{deact} on $R_{deact}^{c}/R_{deact}^{nc}$ are however negligible, consistent with the fairly minor difference in $\bar{n}_{CuCl_2}$ between cases A and B (Figure 7c).

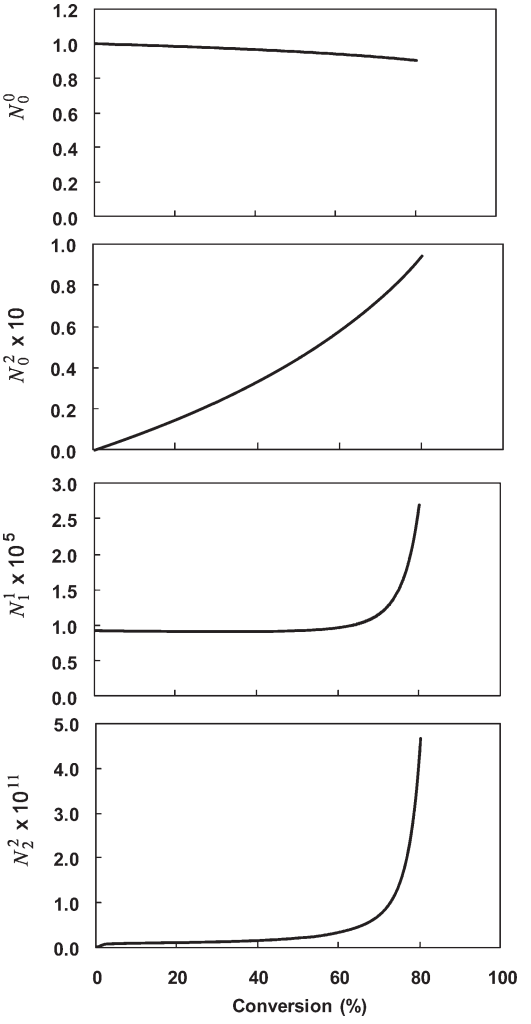

Figure 9. Simulated fractions of particles N_i^j (the number fraction of particles with i P$^\bullet$ and j CuCl$_2$) as functions of conversion for St/polystyrene-Cl/CuCl/dNbpy in a dispersed system with $d = 30$ nm at 75 °C. Conversion-dependent k_t and k_{deact} (case A; see text) and $k_{i,th} = 0$.

To further probe the effects of compartmentalization on deactivation, the individual values of R_{deact}^{c} and R_{deact}^{nc} were examined for case A in the absence of spontaneous initiation for $d = 30$ nm. Figure 11 shows the compartmentalized (Figure 11a) and noncompartmentalized (Figure 11b) deactivation rates vs conversion. R_{deact}^{c} remains constant to high conversion despite the significant changes in k_{deact}, $\bar{n}_{P^\bullet}$, and $\bar{n}_{CuCl_2}$ with conversion. Deactivation can occur in the particles N_1^1, N_1^3, N_2^2, and N_2^4 (as well as in particles of higher i and j), but $N_1^1 \gg N_1^3$, N_2^2, and N_2^4, and consequently R_{deact}^{c} is determined by deactivation in particles of type N_1^1. A deactivation event in a particle of type N_1^1 is the result of two events that occur in series: activation to generate a particle of the type N_1^1 followed by rapid deactivation. The former is the rate-determining step, which is why the decrease in k_{deact} at high conversion is not affecting R_{deact}^{c}, which remains constant. R_{deact}^{nc} (Figure 11b) can be explained in a trivial fashion—it increases with increasing conversion as a result of the conversion dependences of k_{deact}, $\bar{n}_{P^\bullet}$, and $\bar{n}_{CuCl_2}$.

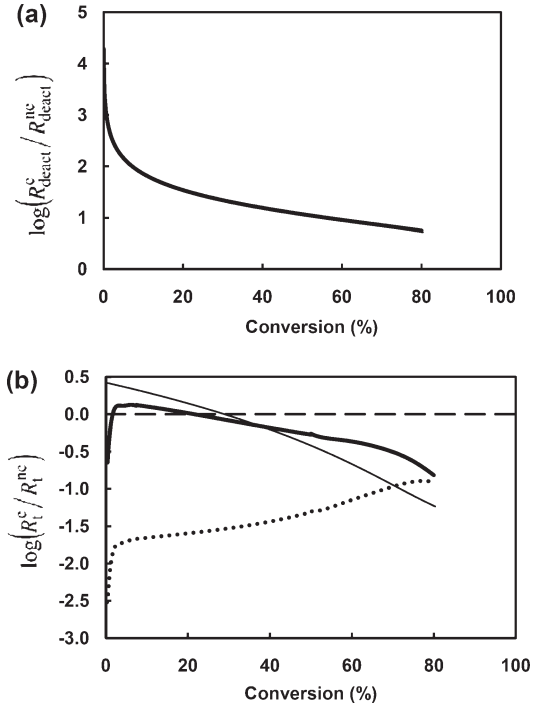

Figure 10. Ratios of simulated "compartmentalized" and "noncompartmentalized" deactivation (a) and termination (b; full lines: $k_{i,th} = 1.12 \times 10^{-12}$ M^{-2} s^{-1}; dotted line: $k_{i,th} = 0$) rates as functions of conversion for St/polystyrene-Cl/CuCl/dNbpy in a dispersed system with $d = 30$ nm at 75 °C. Thick lines: conversion-dependent k_t and k_{deact} (case A; see text). Thin lines: $k_t = 1.2 \times 10^8$ M^{-1} s^{-1} and $k_{deact} = 4.3 \times 10^6$ M^{-1} s^{-1} (case B). The two lines are superimposed in (a). The broken line in (b) indicates $R_t^c = R_t^{nc}$.

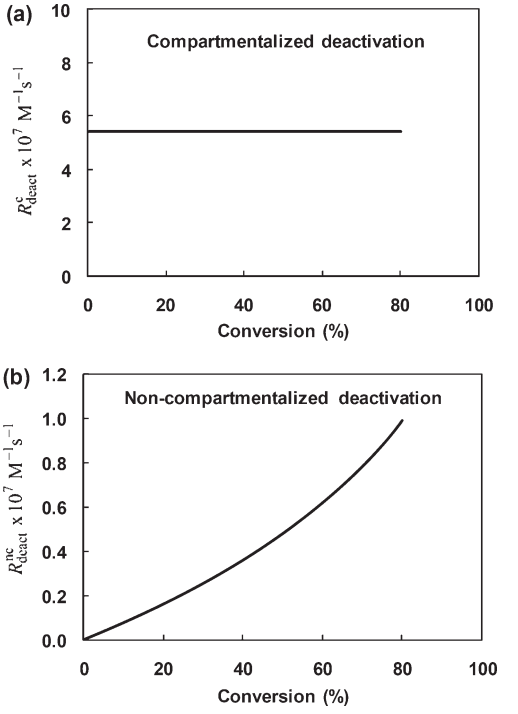

Figure 11. Simulated "compartmentalized" (a) and "noncompartmentalized" (b) deactivation rates as functions of conversion for St/polystyrene-Cl/CuCl/dNbpy in a dispersed system with $d = 30$ nm at 75 °C. Conversion-dependent k_t and k_{deact} (case A; see text) and $k_{i,th} = 0$.

.Figure 10b shows the values of R_t^c/R_t^{nc} for termination. Both case A and case B reveal a gradual decrease in R_t^c/R_t^{nc} with increasing conversion (except for the initial increase in case A—explained below). Spontaneous initiation of St[39,40] generates radicals in pairs, and the rate of geminate termination of these radicals increases with decreasing particle size due to the confined space effect. In the model, the overall termination rate is the sum of all radical−radical coupling reactions (except deactivation), and for sufficiently small particles, the increase in geminate termination rate of spontaneously generated radicals outweighs the reduction in termination by segregation of radicals generated from activation of PCl. This explains why $R_t^c > R_t^{nc}$ at low conversion. The rate of spontaneous initiation is proportional to [St]^3, and thus it decreases strongly with increasing conversion. It follows that the contribution of geminate termination toward the overall termination rate decreases with increasing conversion, and therefore R_t^c/R_t^{nc} decreases with increasing conversion. To illustrate this point, simulations were repeated for case A without spontaneous initiation, revealing how $R_t^c/R_t^{nc} < 1$ throughout the conversion range investigated. As conversion increases, R_t^c/R_t^{nc} (with spontaneous initiation) approaches R_t^c/R_t^{nc} (without spontaneous initiation), and at 80% conversion, the values are very similar, illustrating the diminishing effect of spontaneous initiation at high conversion (Figure 10b).

Figure 12 shows R_t^c (Figure 12a) and R_t^{nc} (Figure 12b) vs conversion for case A for $d = 30$ nm in the absence of spontaneous initiation. The value of R_t^c remains approximately constant to ~60% conversion, beyond which it increases significantly. The decrease in k_t with conversion (Figure 1) only has a very small effect on R_t^c as evidenced by simulations with $k_t = 1.2 \times 10^8$ M^{-1} s^{-1} yielding very similar

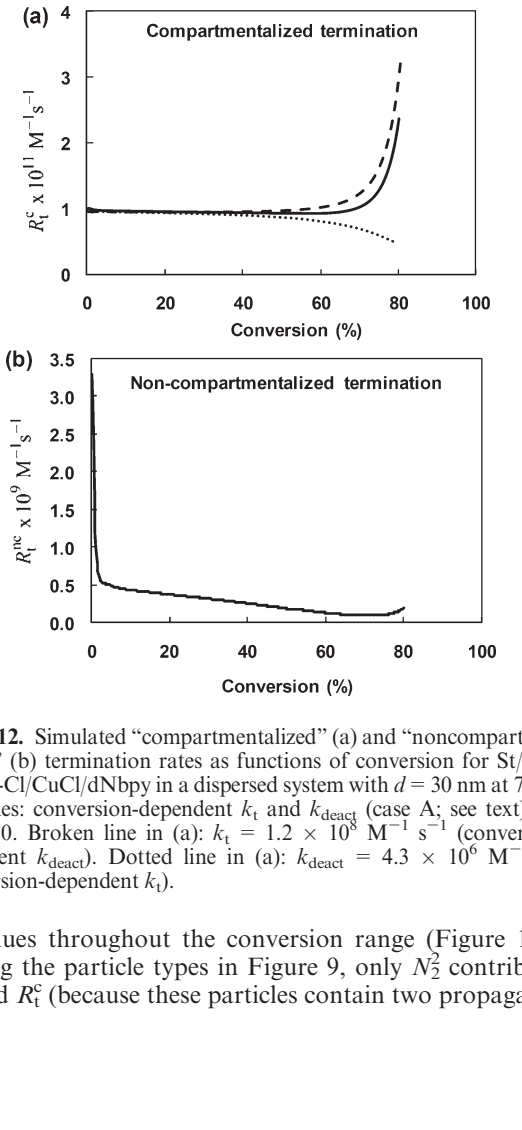

Figure 12. Simulated "compartmentalized" (a) and "noncompartmentalized" (b) termination rates as functions of conversion for St/polystyrene-Cl/CuCl/dNbpy in a dispersed system with $d = 30$ nm at 75 °C. Full lines: conversion-dependent k_t and k_{deact} (case A; see text) and $k_{i,th} = 0$. Broken line in (a): $k_t = 1.2 \times 10^8$ M^{-1} s^{-1} (conversion-dependent k_{deact}). Dotted line in (a): $k_{deact} = 4.3 \times 10^6$ M^{-1} s^{-1} (conversion-dependent k_t).

R_t^c values throughout the conversion range (Figure 12a). Among the particle types in Figure 9, only N_2^2 contributes toward R_t^c (because these particles contain two propagating

radicals that can terminate), and the conversion profile of N_2^2 closely correlates with the conversion profile of R_t^c. The reason that the value of k_t only has a marginal effect is that R_t^c is largely determined by the value of N_2^2, which is dictated by k_{act}, k_{deact}, and k_t. Particles of type N_2^2 are mainly generated by an activation event occurring in a particle of type N_1^1, which are in turn generated by activation in N_0^0. In particles N_1^1, deactivation is much more likely than an activation event. For $d = 30$ nm, the activation time is given by $(N_A \nu_p k_{act}[PCl])^{-1} = 3.91$ s; i.e., an activation event occurs every 3.91 s in any given particle. The time taken for deactivation to occur in a particle N_1^1 is given by $N_A \nu_p / k_{deact} = 0.001\,97$ s; i.e., the probability of activation occurring in a given N_1^1 particle is only 0.05%. This explains the influence of k_{deact} on generation of N_2^2 and thus on R_t^c. Termination competes with deactivation in particles of type N_2^2, consistent with the fact that simulations with a constant value of $k_{deact} = 4.3 \times 10^6$ M^{-1} s^{-1} (as opposed to k_{deact} decreasing at high conversion) does not result in the increase in R_t^c at high conversion (Figure 12a). The decrease in k_{deact} at high conversion results in an increase in particles N_1^1 and N_2^2 and thus also an increase in R_t^c. The value of k_{deact} therefore affects R_t^c not only via competition of deactivation with termination in particles N_2^2 but also by affecting the value of N_1^1.

The deactivation rate obviously influences the termination rate also in the noncompartmentalized system, but in this case the situation is much simpler. A reduction in R_{deact}^{nc} results in an increase in $[P^\bullet]$ and consequently an increase in R_t^{nc}. The values of R_t^{nc} displayed in Figure 12b can thus be readily explained based on the conversion dependences of k_t and $\overline{n}_{P\bullet}$ ($[P\bullet] = \overline{n}_{P\bullet}/N_A \nu_p$). The sharp initial decrease corresponds to the decrease in k_t and explains the initial increase in R_t^c/R_t^{nc} in Figure 10b for case A. The increase in R_t^{nc} at high conversion is less significant than for R_t^c because the decrease in k_{deact} is more strongly counteracted by the decrease in k_t.

Conclusions

Compartmentalization effects to high conversion have been investigated in the ATRP system styrene/polystyrene-Cl/CuCl/4,4′-di(5-nonyl)-2,2′-bipyridine (dNbpy) at 75 °C by use of modeling and simulations employing modified Smith−Ewart equations in connection with conversion-dependent rate coefficients.

The behavior is qualitatively the same as previously reported in ATRP and NMP at low conversion; i.e., R_p is lower than in bulk for sufficiently small particles but higher than in bulk for a certain particle size range. The region with lower R_p than in bulk is associated with better control (lower M_w/M_n), whereas the higher R_p region is associated with poorer control than in bulk. The livingness is improved relative to bulk in both regions. Segregation of propagating radicals causes improved livingness, whereas the confined space effect on deactivation results in better control.

The effects of conversion-dependent k_{deact} and k_t were investigated in detail for $d = 30$ nm. For this particular system, the vast majority of particles contain no propagating radicals and no deactivator species ($CuCl_2$), and hence most activation events generate particles of the type N_1^1. The conversion dependence of k_t results in a slight increase in livingness at high conversion relative to when k_t remains constant. The decrease in k_{deact} at high conversion results in an increase in the number of monomer units added per activation−deactivation cycle, thus giving a slight loss of control relative to when k_{deact} remains constant.

Despite significant changes in k_{deact}, $\overline{n}_{P\bullet}$, and $\overline{n}_{CuCl_2}$ with conversion, the compartmentalized overall deactivation rate (R_{deact}^c) remains constant to high conversion, which may seem to contradict the preceding sentence. However, for example, if a dormant chain is in the active state twice during a given time period, then R_{deact}^c (considering this chain only) is unaltered by a change in the length of time the chain is in the active state (which is dictated by k_{deact}); i.e., it is possible to have different numbers of monomer units added per activation−deactivation cycle for the same R_{deact}^c. The origin of the constancy of R_{deact}^c is that deactivation is a result of two events in series: activation to generate a particle of the type N_1^1 followed by rapid deactivation, the former of which is the rate-determining step. The situation is similar with regards to termination—the value of k_t only has a minor effect on the compartmentalized termination rate (R_t^c) because R_t^c is strongly influenced by the number of particles of type N_2^2 (where termination predominantly occurs), which in turn is dictated to a large extent by k_{act} and k_{deact}.

The results presented are, from a quantitative viewpoint, specific to the system/conditions investigated. However, in a qualitative sense, the findings are expected to apply to ATRP in dispersed systems in general, although it must be borne in mind that the conversion dependences of k_{deact} and k_t may vary significantly between systems. The present results further illustrate how particle size can potentially be exploited to improve both control and livingness in ATRP in dispersed systems.

Acknowledgment. The author is grateful to Prof. C. Barner-Kowollik (Karlsruhe Institute of Technology, Germany) for providing experimental data on k_t conversion- and chain-length dependence.

References and Notes

(1) Braunecker, W. A.; Matyjaszewski, K. *Prog. Polym. Sci.* **2007**, *32*, 93–146.
(2) Zetterlund, P. B.; Kagawa, Y.; Okubo, M. *Chem. Rev.* **2008**, *108*, 3747–3794.
(3) Cunningham, M. F. *Prog. Polym. Sci.* **2008**, *33*, 365–398.
(4) Zetterlund, P. B.; Aldabbagh, F.; Okubo, M. *J. Polym. Sci., Part A: Polym. Chem.* **2009**, *47*, 3711–3728.
(5) Oh, J. K.; Bencherif, S. A.; Matyjaszewski, K. *Polymer* **2009**, *50*, 4407–4423.
(6) Hawker, C. J.; Wooley, K. L. *Science* **2005**, *309*, 1200–1205.
(7) Boyer, C.; Bulmus, V.; Davis, T. P.; Ladmiral, V.; Liu, J.; Perrier, S. *Chem. Rev.* **2009**.
(8) Zetterlund, P. B.; Okubo, M. *Macromolecules* **2006**, *39*, 8959–8967.
(9) Fischer, H. *Chem. Rev.* **2001**, *101*, 3581–3610.
(10) Georges, M. K.; Veregin, R. P. N.; Kazmaier, P. M.; Hamer, G. K. *Macromolecules* **1993**, *26*, 2987–2988.
(11) Kamigaito, M.; Ando, T.; Sawamoto, M. *Chem. Rev.* **2001**, *101*, 3689–3745.
(12) Matyjaszewski, K.; Xia, J. H. *Chem. Rev.* **2001**, *101*, 2921–2990.
(13) Moad, G.; Rizzardo, E.; Thang, S. H. *Aust. J. Chem.* **2006**, *59*, 669–692.
(14) Barner-Kowollik, C. *Handbook of RAFT Polymerization*; Wiley-VCH: New York, 2008.
(15) Luo, Y.; Wang, R.; Yang, L.; Li, B.; Zhu, S. *Macromolecules* **2006**, *39*, 1328–1337.
(16) Tobita, H. *Macromol. Theory Simul.* **2009**, *18*, 108–119.
(17) Zetterlund, P. B. *Macromol. Theory Simul.* **2009**, in press.
(18) Zetterlund, P. B.; Okubo, M. *Macromol. Theory Simul.* **2007**, *16*, 221–226.
(19) Zetterlund, P. B.; Okubo, M. *Macromol. Theory Simul.* **2009**, *18*, 277–286.
(20) Tobita, H. *Macromol. Theory Simul.* **2007**, *16*, 810–823.
(21) Kagawa, Y.; Zetterlund, P. B.; Minami, H.; Okubo, M. *Macromol. Theory Simul.* **2006**, *15*, 608–613.
(22) Zetterlund, P. B.; Kagawa, Y.; Okubo, M. *Macromolecules* **2009**, *42*, 2488–2496.
(23) Charleux, B. *Macromolecules* **2000**, *33*, 5358–5365.
(24) Delaittre, G.; Charleux, B. *Macromolecules* **2008**, *41*, 2361–2367.
(25) Kagawa, Y.; Zetterlund, P. B.; Minami, H.; Okubo, M. *Macromolecules* **2007**, *40*, 3062–3069.
(26) Simms, R. W.; Cunningham, M. F. *Macromolecules* **2007**, *40*, 860–866.

(27) Simms, R. W.; Cunningham, M. F. *Macromolecules* **2008**, *41*, 5148–5155.
(28) Maehata, H.; Buragina, C.; Cunningham, M.; Keoshkerian, B. *Macromolecules* **2007**, *40*, 7126–7131.
(29) Wakamatsu, J.; Kawasaki, M.; Zetterlund, P. B.; Okubo, M. *Macromol. Rapid Commun.* **2007**, *28*, 2346–2353.
(30) Zetterlund, P. B.; Wakamatsu, J.; Okubo, M. *Macromolecules* **2009**, *42*, 6944–6952.
(31) Shipp, D. A.; Matyjaszewski, K. *Macromolecules* **1999**, *32*, 2948–2955.
(32) Zetterlund, P. B.; Yamazoe, H.; Yamada, B.; Hill, D. J. T.; Pomery, P. J. *Macromolecules* **2001**, *34*, 7686–7691.
(33) Buback, M.; Egorov, M.; Gilbert, R. G.; Kaminsky, V.; Olaj, O. F.; Russell, G. T.; Vana, P.; Zifferer, G. *Macromol. Chem. Phys.* **2002**, *203*, 2570–2582.
(34) Yamazoe, H.; Yamada, B.; Zetterlund, P. B.; Hill, D. J. T.; Pomery, P. J. *Macromol. Chem. Phys.* **2001**, *202*, 824.
(35) Delgadillo-Velazquez, O.; Vivaldo-Lima, E.; Quintero-Ortega, I. A.; Zhu, S. *AlChE J.* **2002**, *48*, 2597–2608.
(36) Wang, A. R.; Zhu, S. *Macromolecules* **2002**, *35*, 9926–9933.
(37) Roa-Luna, M.; Nabifar, A.; McManus, N. T.; Vivaldo-Lima, E.; Lona, L. M. F.; Penlidis, A. *J. Appl. Polym. Sci.* **2008**, *109*, 3665–3678.
(38) Goto, A.; Fukuda, T. *Prog. Polym. Sci.* **2004**, *29*, 329–385.
(39) Hui, A. W.; Hamielec, A. E. *J. Appl. Polym. Sci.* **1972**, *16*, 749–769.
(40) Khuong, K. S.; Jones, W. H.; Pryor, W. A. *J. Am. Chem. Soc.* **2005**, *127*, 1265–1277.
(41) Butte, A.; Storti, G.; Morbidelli, M. *DECHEMA Monogr.* **1998**, *134*, 497–507.
(42) Heath, M. T. *Scientific Computing, An Introductory Survey*, 2nd ed.; McGraw-Hill: New York, 2002.
(43) Taylor, P. *Adv. Colloid Interface Sci.* **1998**, *75*, 107–163.
(44) Atkins, P. W.; de Paula, J. *Physical Chemistry*; Oxford University Press: Oxford, UK, 2006.
(45) Zetterlund, P. B.; Yamazoe, H.; Yamada, B. *Macromol. Theory Simul.* **2003**, *12*, 379–385.
(46) Buback, M.; Gilbert, R. G.; Hutchinson, R. A.; Klumperman, B.; Kuchta, F. D.; Manders, B. G.; ÒDriscoll, K. F.; Russell, G. T.; Schweer, J. *Macromol. Chem. Phys.* **1995**, *196*, 3267–3280.
(47) Barner-Kowollik, C.; Russell, G. T. *Prog. Polym. Sci.* **2009**, *34*, 1211−1259.
(48) Vana, P.; Davis, T. P.; Barner-Kowollik, C. *Macromol. Rapid Commun.* **2002**, *23*, 952–956.
(49) Faldi, A.; Tirrell, M.; Lodge, T. P.; von-Meerwall, E. *Macromolecules* **1994**, *27*, 4184–4192.
(50) Scheren, P.; Russell, G. T.; Sangster, D. F.; Gilbert, R. G.; German, A. L. *Macromolecules* **1995**, *28*, 3637–3649.
(51) D'hooge, D. R.; Reyniers, M. F.; Marin, G. B. *Macromol. React. Eng.* **2009**, *3*, 185–209.
(52) Buback, M.; Kowollik, C.; Kurz, C.; Wahl, A. *Macromol. Chem. Phys.* **2000**, *201*, 464–469.